Proceedings of Global Power and Propulsion Society
ISSN-Nr: 2504-4400
GPPS Xi'an21
18th – 20th October, 2021
www.gpps.global

# GPPS-TC-2021-NO.16

# PRESSURE FLUCTUATION CHARACTERISTICS OF MIXED-FLOW PUMP UNDER NEAR STALL CONDITION

**Wei Li**
**Jiangsu University**
lwjiangda@ujs.edu.cn
Zhenjiang, Jiangsu, China

**Dele Lu**
**Jiangsu University**
2523057045@qq.com
Zhenjiang, Jiangsu, China

**Leilei Ji**
**Jiangsu University**
jileileidemail@163.com
Zhenjiang, Jiangsu, China

**Ling Zhou**
**Jiangsu University**
lingzhou@ujs.edu.cn
Zhenjiang, Jiangsu, China

**Ramesh K. Agarwal**
**Washington University in St. Louis**
rka@wustl.edu
St. Louis, Missouri, US

## ABSTRACT

When the rotating stall occurs in a mixed-flow pump, the periodic generation and disappearance of the stall core often cause unstable pressure pulsation. Based on the *k-ε* turbulence model, the time domain and frequency domain responses of the pressure fluctuation of the mixed-flow pump with 3 kinds of different flange clearances are studied. The results show that the time-domain curves of pressure fluctuation at each monitoring point show periodic changes near stall condition, but the peak and trough characteristics of impeller rotation are not obvious. There is a large phase difference between adjacent monitoring points, accompanied by a strong pressure drop. When the flange clearance is 0.5 mm and 0.8 mm, the time domain curve of pressure fluctuation has 2 wave troughs in one cycle. In the near stall condition, the main frequency of pressure fluctuation at 3 monitoring points in the same channel is 0.2 times the rotational frequency, i.e. stall frequency. In addition, the main frequency amplitude in the middle of the outlet is the largest, and the larger the gap is, the larger the main frequency amplitude is.

## INTRODUCTION

Due to the advantages of large flow, high efficiency, and good cavitation resistance, mixed-flow pump plays an important role in national infrastructure construction and is widely used in water conservancy engineering, agricultural irrigation, sewage treatment, ship propulsion, aerospace, and other application engineering fields[1-5]. However, when the pump is operating under off-design conditions, stall mass is easy to occur in the impeller due to the increase of blade angle of attack[6]. The continuous generation and shedding of stall mass often induce low-frequency pressure pulsation, which makes the noise and vibration of the pump increase. When the stall vortex frequency is consistent with the natural frequency of the unit, it will also cause the vibration of the whole unit and seriously threaten the safe and stable operation of the unit[7,8].

In recent years, the pressure fluctuation of the mixed-flow pump under off-design conditions has been paid attention by scholars at home and abroad. With the development of CFD, the application of the numerical method has become an important auxiliary means to study the internal pressure pulsation of the pump and explore the correlation between pressure pulsation and internal flow. Jin et al.[9] used Fluent to simulate the internal flow field of the mixed-flow pump. By analyzing the internal pressure fluctuation characteristics, it was concluded that with the decrease of the flow rate, the pressure fluctuation increased, and the pressure fluctuation amplitude at the impeller inlet was the largest. At the same time, the pressure fluctuation frequency at the impeller inlet and outlet was the impeller blade frequency, and the dominant frequency at the guide vane inlet and outlet changed with the change of the flow rate. The unsteady pressure pulsation in turbomachinery can be caused by the change of flow pattern, dynamic and static interference, and rotating stall. Byskov et al.[10] found the stall zone in the flow passage of the mixed-flow pump through large eddy simulation, and there was also a recirculation zone in the working face of the impeller. Yamade et al.[11] also found through large eddy simulation that

when rotating stall occurs in the mixed-flow pump, the flow pattern inside the pump becomes very unstable, and there is a local high-pressure region at the outlet flange on the back of the impeller blade, and flow separation occurs. Du et al.[12] carried out the large eddy simulation of the full three-dimensional flow passage in the guide vane mixed-flow pump, and analyzed the time-frequency characteristics of the pressure fluctuation at eight monitoring points of the impeller inlet and outlet section. It was found that the amplitude of the pressure fluctuation coefficient at the monitoring point at the outlet was larger than that at the inlet, and the attenuation speed of the pressure fluctuation was slower under the action of the rotating stall, flow separation effect, and static guide vane interference. Li et al.[13,14] studied the influence of dynamic and static interference on the internal pressure fluctuation characteristics of low specific speed mixed-flow pump by simulating the internal flow field. The results show that the amplitude of pressure fluctuation in the impeller and at the flange of the impeller outlet reaches the maximum, and the pressure fluctuation increases gradually from the impeller inlet to the guide vane outlet. And it is found that when the rotating stall occurred in the mixed-flow pump, unstable vortices appeared at the inlet of the impeller and caused the blockage of the flow passage. The vortices almost occupied the whole inlet flow passage, which caused the deterioration of the inlet flow pattern. Zhang et al.[15] analyzed the internal flow field and pressure fluctuation characteristics of the mixed-flow pump under different working conditions. The results show that when the rotating stall occurs, a large number of vortices appear near the suction surface of the guide vane, the vortex size increases first and then decreases along the guide vane passage, and the pressure fluctuation at the vortex core is the smallest. The amplitude of pressure fluctuation in the impeller from hub to rim increases gradually, and the frequency distribution of pressure fluctuation at the inlet and outlet of the impeller is similar.

In the aspect of experimental research, Miyabe et al. [16,17] used PIV test and numerical method to analyze the phenomenon of large-scale secondary reflux and vortex flow from the inlet of guide vane to the outlet of mixed-flow pump impeller under small flow condition, and clarified that the rotating stall of guide vane under small flow condition is the main reason for inducing the unstable characteristics of the mixed-flow pump. At the same time, the rotating stall at the inlet of the guide vane also makes the pressure pulsation fluctuate periodically. Zhang et al.[14] studied the internal pressure pulsation characteristics and laws of high specific speed mixed-flow pump under different working conditions by experimental methods. The results show that under different flow conditions, the amplitude of pressure pulsation from impeller inlet to guide vane outlet decreases in turn, and the periodic fluctuation of pressure pulsation also decreases in turn. Under the condition of small flow rate, the pressure fluctuation at impeller outlet and guide vane outlet is relatively weak due to the influence of low-frequency large-scale vortex generated by flow separation and stall, tip leakage flow, and backflow.

At present, there are many researches on the pressure pulsation in the pump at home and abroad, but the research on the pressure pulsation of the mixed-flow pump under stall conditions is very rare. Therefore, the author takes the guide vane mixed-flow pump as the research object, and studies the influence of near stall condition on the pressure pulsation of the mixed-flow pump under three different flange clearances by numerical simulation method, revealing the internal pressure pulsation law of mixed-flow pump under stall condition. The research results have important reference value for the design and operation of the mixed-flow pump in large pumping station.

## METHODOLOGY

### Simulation Model and Grid Generation

The research object of this paper is the guide vane mixed-flow pump, and its design parameters are as follows: rated flow $Q_{des}$ = 380 m$^3$/h, head $H$ = 6 m, speed $n$ = 1 450 r/min, specific speed $n_s$ = 480, blade number $Z$ = 4, guide vane number $Z_d$ = 7. The mixed-flow pump model includes inlet section, impeller section, guide vane section, annular volute chamber, and outlet section, as shown in Figure 1. In the study, to keep the runner chamber size unchanged, the flange clearance was changed by changing the impeller diameter. The 3 groups of flange clearances were 0.2 mm, 0.5 mm, and 0.8 mm, respectively.

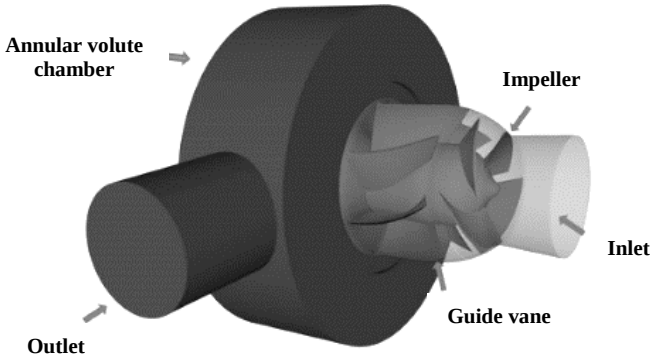


**Figure 1 Mixed-flow pump 3D model**

The grid quality has a direct impact on the reliability of the calculation results. Therefore, ICEM CFD software is used to divide 5 different water regions into more precise hexahedral structured grids. The y-block topology is used in the inlet section, and the J/O-type topology and H/O-type topology are used in the impeller water domain and guide vane water domain respectively. In order to obtain high-quality flange gap area grid to meet the requirements of wall function, the internal grid of flange gap is encrypted by increasing the number of nodes, and the transition section from gap to impeller is encrypted to ensure uniform transition. It is found that when the number of global grids is close to 4.91 million, the head change of the mixed-flow pump calculated by increasing the number of grids by densifying the grid is small, and the relative error is within ±5%, which meets the requirements of grid independence test. Figure 2 and Figure 3 show the global mesh and the encrypted mesh near the rim region respectively.

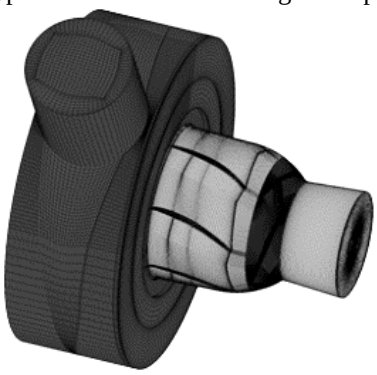

**Figure 2 Global grid**

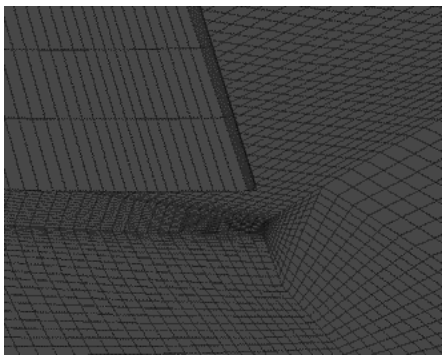

**Figure 3 Rim area grid**

### Turbulence Model and Boundary Conditions

Based on the Reynolds time-averaged Navier-Stokes equations, the $k$-$\varepsilon$ turbulence model is used to discretize the equations by the finite volume method and SIMPLEC algorithm, and the second-order upwind scheme is adopted. For the setting of boundary conditions, the inlet boundary is the pressure inlet, which is 20 kPa, and the outlet boundary is the mass flow outlet, which is set according to the change of flow. The wall function is non-slip wall, and the reference pressure is 101.325 kPa, and the convergence accuracy is set to $10^{-5}$. In the unsteady calculation, the total calculation step is set as 2 000 steps, the calculation time step is 3°, and it is saved once every 10 steps. The above settings and numerical calculations are carried out by commercial software ANSYS CFX.

## RESULTS AND DISCUSSION

### Experimental Verification of External Characteristic

Due to the limitation of the test conditions, the head and efficiency of the mixed-flow pump with 0.5 mm and 0.8 mm flange clearance were measured and compared with the simulation results. It can be seen from Figure 4 that the positive slope of the $H$-$Q$ curve of the mixed-flow pump is the most obvious when the flange clearance is 0.8 mm. In the flow range from $0.4Q_{des}$ to $1.2Q_{des}$, the numerical simulation results are basically consistent with the experimental results, only when the flow rate is low, there is a large error. In general, the head and efficiency predicted by the numerical simulation are in good agreement with the experimental results, so the reliability of the simulation results is high.

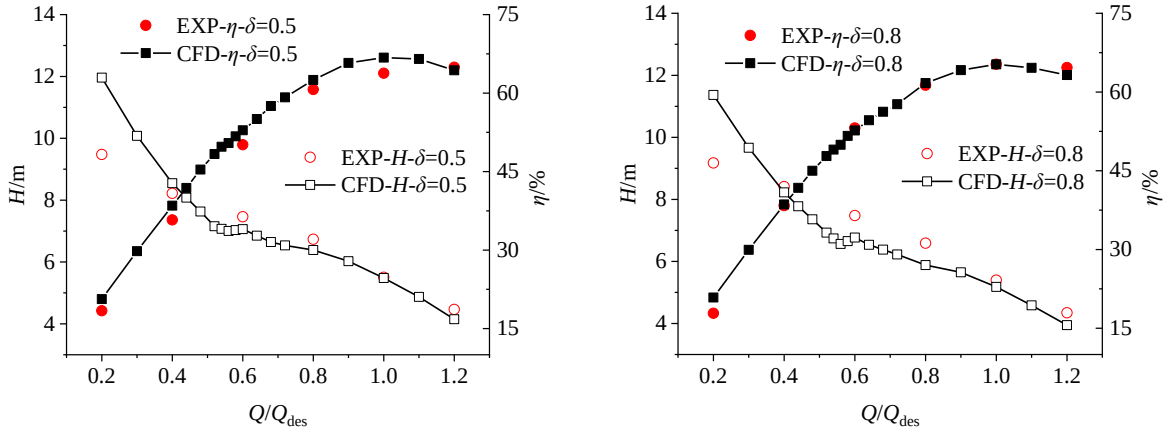


$\delta$=0.5 mm $\delta$=0.8 mm

**Figure 4 Comparison of external characteristic between numerical simulation and test**

### Time-domain analysis of pressure fluctuation under different tip clearances

In the near stall condition, the vortex will gradually form at the outlet of the impeller passage, and its blocking effect is very obvious. With the rotation of the impeller, the vortex will develop and propagate in the opposite direction of the rotation direction of the impeller. In order to study the propagation characteristics of the stall core, monitoring points are set at the outlet of 4 flow channels of the impeller, and the monitoring points in each flow channel are arranged from the hub to the rim, as shown in Figure 5. In order to better analyze the pressure fluctuation at each monitoring point, the pressure coefficient $C_p$ is used to deal with the transient pressure dimensionless, which is used to express the intensity of pressure fluctuation.

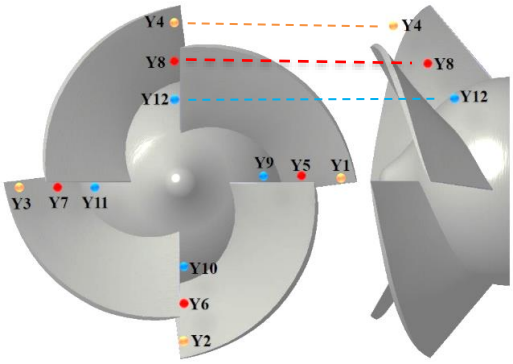


**Figure 5 Position of impeller outlet monitoring points**

Figure 6 shows the time-domain diagram of the pressure fluctuation at the monitoring points Y5, Y6, Y7, and Y8 at the outlet of 4 flow channels of the impeller under near stall condition. It can be seen from the figure that the pressure fluctuation curves of 4 monitoring points along the circumferential direction under 3 different flange clearances show periodic changes under near stall condition, but the peaks and troughs representing the impeller rotation are not obvious. Under the same flange clearance, the pressure fluctuation curve is similar in different channels, but there is a large phase difference between the adjacent monitoring points. With the rotation of the impeller, there will be a strong pressure drop at the monitoring points, which is the main periodic characteristic of the pressure fluctuation curve near stall. When the gap is 0.2 mm, there is only one trough in one cycle of the pressure fluctuation curve. When the gap is 0.5 mm or 0.8 mm, it can be found that there are two troughs in one cycle of the pressure fluctuation curve. Therefore, it can be judged that the number of stall nuclei changes from 1 to 2, and the propagation of double stall nuclei is more complex than that of single stall nuclei in the 2 adjacent channels, so the pressure fluctuation curve is slightly more complex than that of the gap of 0.2 mm. In the adjacent channel, the second pressure drop in the current channel corresponds to the first pressure drop in the next channel. After the exit pressure drop of the current channel, the second pressure drop occurs in the next channel, and the first pressure drop occurs in the flow passage after the next. This process corresponds to a stall vortex propagation process in which the current flow passage exits the stall state, the next flow passage continues to be in the stall state, and the flow passage after next enters the stall state at the same time. Because the double stall nuclei will interfere with each other in the process of propagation, the pressure fluctuation curve will fluctuate slightly when it forms 2 troughs. At the same time, when the gap is 0.5 mm, the phase difference between adjacent monitoring points is almost unchanged, while when the gap is 0.8 mm, the phase difference between adjacent monitoring points is shortened, which indicates that the propagation of stall nuclei is accelerating.

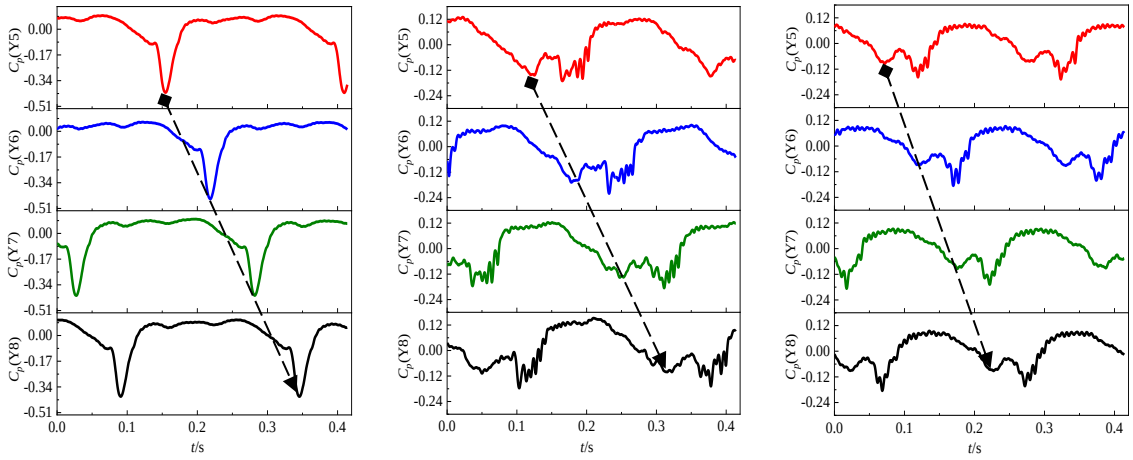


$\delta$=0.2 mm $\delta$=0.5 mm $\delta$=0.8 mm

**Figure 6 Time-domain characteristics of pressure coefficient at Y5, Y6, Y7, Y8**

Figure 7 shows the time domain diagram of pressure fluctuation from the monitoring point of the hub to the monitoring point of the rim in a single channel with different rim clearances under near stall condition. It can be seen from the figure that the pressure fluctuation amplitude of the monitoring point Y8 located in the middle of the impeller outlet is larger, while the pressure fluctuation amplitude of the monitoring point Y4 located in the hub and flange of the impeller outlet is smaller and the difference is not big, but the pressure fluctuation frequency of the monitoring point Y4 located in the flange is higher. It shows that the main part of the vortex is located in the middle of the impeller outlet, which has the greatest influence on the pressure fluctuation. At the same time, when the gap is larger than 0.2 mm, the lowest value of the pressure fluctuation curve increases, which indicates that the two stall nuclei in the adjacent channel interfere with each other in the propagation process.

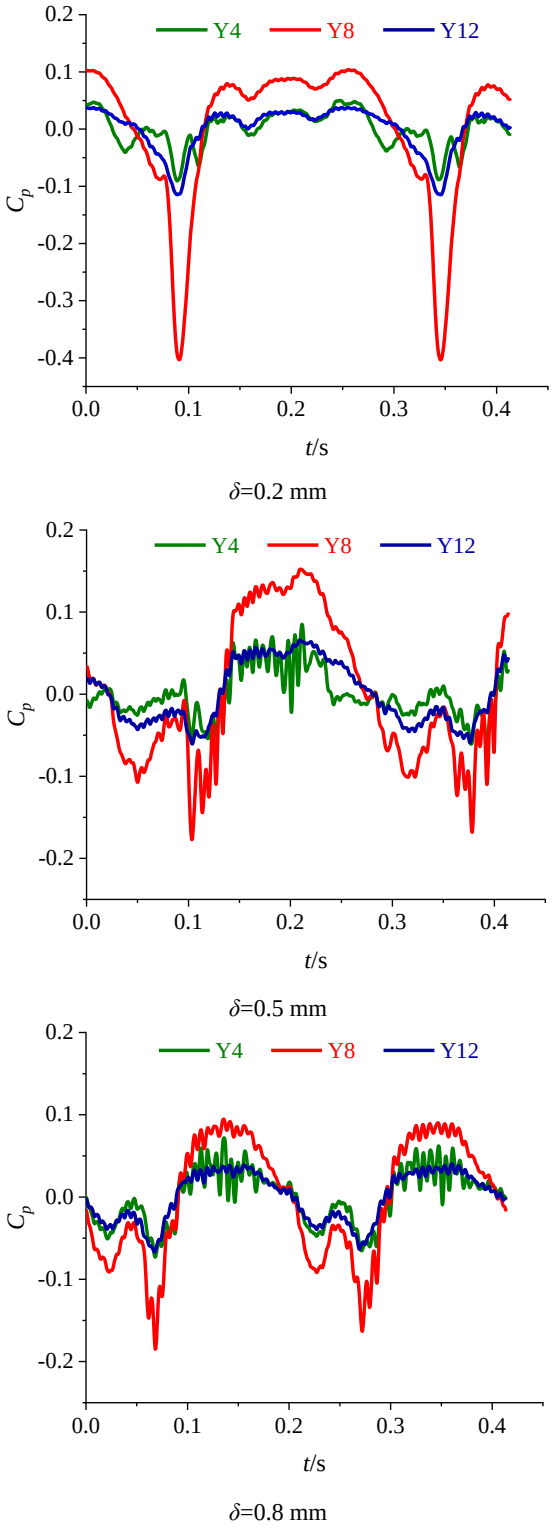


**Figure 7 Time-domain characteristics of pressure coefficient at Y4, Y8, Y12**

### Frequency domain analysis of pressure fluctuation under different tip clearances

In order to analyze the frequency-domain characteristics of pressure fluctuation, the fast Fourier transform (FFT) is used to transform the time-domain information into the frequency-domain information. Figure 8 shows the frequency domain diagram of pressure pulsation at 3 monitoring points from hub to rim in a single flow passage of impeller under near stall condition, where abscissa $f^*$ is the multiple of impeller rotation frequency. It can be seen from the figure that the main frequency of the frequency domain curve of pressure fluctuation at the 3 monitoring points is not the impeller rotation frequency or blade frequency, but 0.2 times of the rotation frequency, and the amplitude of the main frequency is high, which is the stall frequency. At the same time, the main frequency amplitude of the monitoring point Y8 located in the middle of the impeller outlet is the largest, while the main frequency amplitude of the monitoring points Y12 and Y4 located in the hub and flange is smaller and the difference is not significant.This is because the main part of the stall core is located in the middle of the impeller outlet, so it has the greatest impact on the pressure fluctuation of the fluid there, and has less impact on the pressure fluctuation of the fluid at the hub and flange.

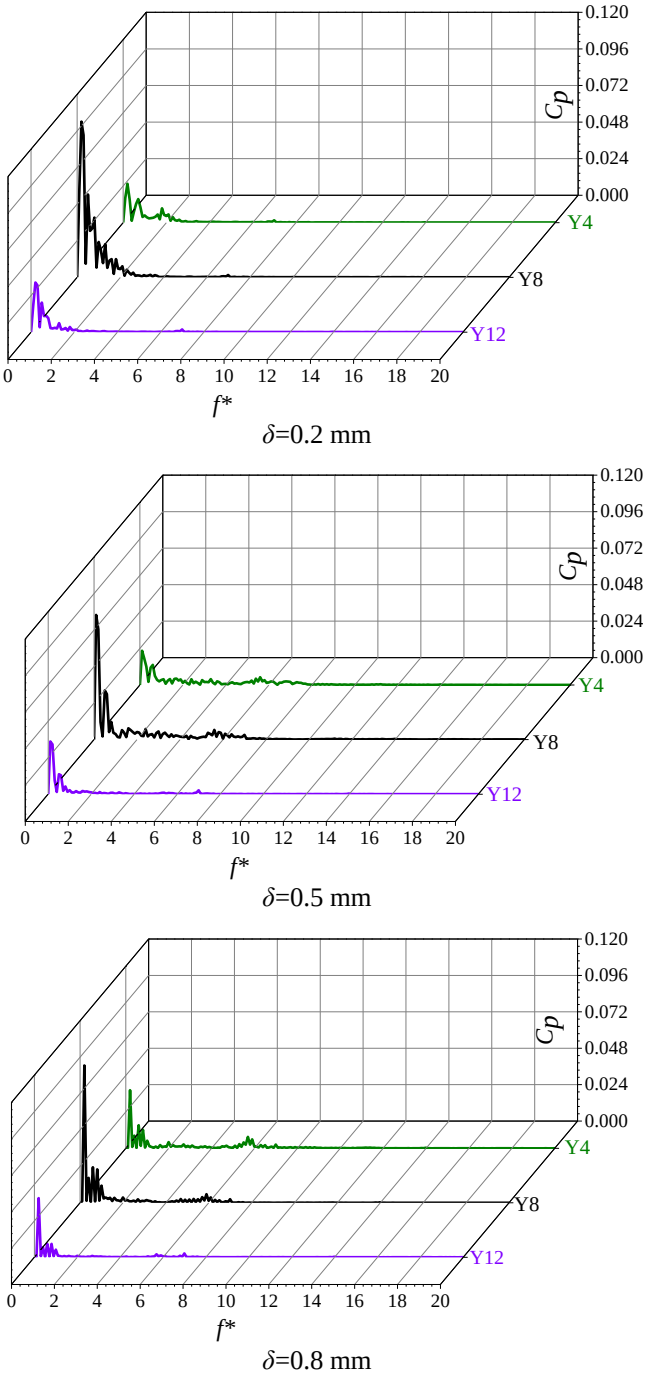


**Figure 8 Frequency domain characteristics of pressure coefficient at Y4, Y8, Y12**

In the near stall condition, the frequency-domain curves of pressure fluctuation at the 3 monitoring points are different due to the different flange clearance, which indicates that the stall state in the impeller is different. Because the main part of the stall core is located in the middle of the impeller outlet, the influence on the frequency-domain curves of pressure fluctuation at the monitoring points is always the most obvious. When the flange clearance is 0.2 mm, the main frequency amplitude of Y8 frequency domain curve at the impeller outlet monitoring point is larger, and the main frequency attenuation is slow. When the gap increases to 0.5 mm, because there are 2 stall cores, compared with the single-channel propagation mode, the pressure drop amplitude is weaker, so the amplitude of the main frequency decreases and the attenuation of the main frequency is faster. In addition, the secondary frequency components on the frequency-domain curve are increased compared with the gap of 0.2 mm, which is also caused by the mutual interference between the 2 stall nuclei. When the flange clearance is 0.8 mm, there are still 2 stall cores, so the overall trend of frequency-domain curve is similar to that when the clearance is 0.5 mm, but the main frequency amplitude increases.

## CONCLUSIONS

In the near stall condition, the time domain curves of pressure fluctuation at each monitoring point show periodic changes, but the characteristics of the peaks and troughs representing the impeller rotation are fuzzy. There is a large phase difference between adjacent monitoring points, and there is a strong pressure drop on the time domain curve, which is the main periodic characteristic of the pressure fluctuation curve near stall.

The phase difference between the adjacent monitoring points is consistent with the propagation period of the stall core under different wheel gaps. With the increase of the gap, the number of stall nuclei increases, and the propagation mechanism of stall nuclei tend to be complex, resulting in 2 wave troughs in one cycle of the pressure fluctuation time domain curve. In addition, since the main part of the vortex is located in the middle of the impeller outlet, the pressure fluctuation of Y8 is the largest.

In the near stall condition, the amplitudes of pressure fluctuation frequency-domain curves at 3 monitoring points in the same channel are quite different, but the main frequency is 0.2 times the impeller rotation frequency, i.e. stall frequency. In addition, the main frequency amplitude of the frequency-domain curve of the middle monitoring point Y8 is the largest. When the number of stall cores is the same, the larger the gap is, the larger the main frequency amplitude is.

## NOMENCLATURE

| | |
|---|---|
| $Q$ | Design Flow Rate |
| $H$ | Head |
| $Z$ | Number of Impeller Blades |
| $Z_d$ | Number of Guide Vane Blades |
| $N$ | Rated Speed |
| $n_s$ | Specific Speed |
| $\eta$ | Efficiency |
| $\delta$ | Flange Clearance |
| $f^*$ | Multiple of Impeller Rotation Frequency |
| $C_p$ | Pressure Coefficient |

## ACKNOWLEDGMENTS

The authors would like to acknowledge CFD Lab of the Washington University in St. Louis for their support. This work was sponsored by the National Key R&D Program Project (No.2020YFC1512405), National Natural Science Foundation of China (Nos.51679111, 51409127), the Fifth "333 High Level Talented Person Cultivating Project" of Jiangsu Province, "Belt and Road" Innovation Cooperation Project of Jiangsu Province (No.BZ2020068), Independent Innovation Fund Project of Agricultural Science and Technology in Jiangsu Province (No.CX(20)2037), Synergistic Innovation Center of Jiangsu on Modern Agricultural Equipment and Technology (No.4091600014), and Six talent peaks project in Jiangsu Province(JNHB-192).

## REFERENCES

[1] Li, et al. (2020). Mechanism and Propagation Characteristics of Rotating Stall in a Mixed-Flow Pump. *Renewable Energy*, 153, pp. 74-92.

[2] Li, et al. (2020). Numerical Investigation of Energy Loss Mechanism of Mixed-Flow Pump under Stall Condition. *Renewable Energy*, 2021(167), pp. 740-760.

[3] Li, et al. (2019). Effect of Tip Clearance on Rotating Stall in a Mixed-Flow Pump[R]. Phoenix, Arizona, USA, 2019.

[4] Li, et al. (2019). Numerical Simulation of Incipient Rotating Stall Characteristics in a Mixed-Flow Pump, AIAA SciTech 2019, January 7-11, San Diego, California.

[5] Ji, et al. (2020). Diagnosis of Internal Energy Characteristics of Mixed-Flow Pump within Stall Region based on Entropy Production Analysis Model. *International Communications in Heat and Mass Transfer*, 117: 0-104784. SCIE.

[6] Ji, et al. (2020). Influence of Tip Leakage Flow and Inlet Distortion Flow on a Mixed-Flow Pump with Different Tip Clearances within the Stall Condition. *Proceedings of the Institution of Mechanical Engineers - Part A: Journal of Power and Energy*, 234(4), pp. 433-453.
[7] Ji, et al. (2020). Transient Characteristics of Internal Flow Fields of Mixed-Flow Pump with Different Tip Clearances under Stall Condition. *Proceedings of the Institution of Mechanical Engineers, Part A: Journal of Power and Energy*, 2020(1), pp. 1-18.
[8] Yang, et al. (2019). Numerical Investigation on the Unstable Flow at Off-Design Condition in a Mixed-Flow Pump. *Proceedings of the Institution of Mechanical Engineers-Part A: Journal of Power and Energy*, 233(7), pp. 849-865.
[9] Jin, et al. (2013). Pressure Fluctuation of Interior Flow in Mixed-flow Pump. *Transactions of the Chinese Society for Agricultural Machinery*, 44(3), pp. 64-68.
[10] Byskov P., et al. (2003). Flow in a Centrifugal Pump Impeller at Design and Off-Design Conditions—Part II: Large Eddy Simulations. *ASME Journal of Fluids Engineering*, 125, pp. 73-83.
[11] Yamade Y., et al. (2009). Large Eddy Simulation of Internal Flow of a Mixed-Flow Pump. *ASME 2009 Fluids Engineering Division Summer Meeting*. American Society of Mechanical Engineers, pp. 407-416.
[12] Du, et al. (2016). Analysis of Pressure Fluctuations in Impeller of Guide Vane Mixed-flow Pump based on Large Eddy Simulation. *Journal of Xihua University*(*Natural Science Edition*), 35(4), pp. 75-78.
[13] Li, et al. (2013). Numerical Analysis of Pressure Fluctuation in Low Specific Spreed Mixed-flow Pump. *Journal of Drainage and Irrigation Machinery Engineering*, 31(3), pp. 205-209.
[14] Li, et al. (2013). Numerical simulation of unstable characteristics in head curve of mixed-flow pump. *Journal of Drainage and Irrigation Machinery Engineering*. 31(5), pp. 384-389.
[15] Zhang, et al. (2017). Analysis of Instability Flow on Mixed-flow Pump based on LES. *Journal of Drainage and Irrigation Machinery Engineering*, 35(4), pp. 303-308, 318.
[16] Miyabe, M., et al. (2006). Unstable Head-flow Characteristic Generation Mechanism of a Low Specific Speed Mixed-flow Pump. *Journal of Thermal Science*, 15(2), pp. 115-120.
[17] Miyabe, M., et al. (2009). A Behavior of the Diffuser Rotating Stall in a Low Specific Speed Mixed-flow Pump. *Turbomachinery*, 35(1), pp. 113-121.
[18] Zhang, et al. (2019). Tests for Inner Pressure Fluctuation Features in an Oblique Flow Pump with High Ratio Rotating Speed. *Journal of Vibration and Shock*, 38(9), pp. 27-34.